Electronic correlations at paramagnetic (001) and (110) NiO surfaces: Charge-transfer and Mott-Hubbard-type gaps at the surface and subsurface of (110) NiO

I. Leonov [1,2,3,*] and S. Biermann[4,5,6,†]

[1]*M. N. Miheev Institute of Metal Physics, Russian Academy of Sciences, 620108 Yekaterinburg, Russia*
[2]*Institute of Physics and Technology, Ural Federal University, 620002 Yekaterinburg, Russia*
[3]*Skolkovo Institute of Science and Technology, 143026 Moscow, Russia*
[4]*CPHT, CNRS, Ecole Polytechnique, IP Paris, F-91128 Palaiseau, France*
[5]*Collège de France, 11 place Marcelin Berthelot, 75005 Paris, France*
[6]*Department of Physics, Division of Mathematical Physics, Lund University, Professorsgatan 1, 22363 Lund, Sweden*

(Received 23 November 2020; revised 8 March 2021; accepted 11 March 2021; published 7 April 2021)

We explore the interplay of electron-electron correlations and surface effects in the prototypical correlated insulating material, NiO. In particular, we compute the electronic structure, magnetic properties, and surface energies of the (001) and (110) surfaces of paramagnetic NiO using a fully charge self-consistent DFT+ dynamical mean-field theory method. Our results reveal a complex interplay between electronic correlations and surface effects in NiO, with the electronic structure of the (001) and (110) NiO surfaces being significantly different from that in bulk NiO. We obtain a sizable reduction of the band gap at the surface of NiO, which is most significant for the (110) NiO surface. This suggests a higher catalytic activity of the (110) NiO surface than that of the (001) NiO one. Our results reveal a charge-transfer character of the (001) and (110) surfaces of NiO. Most notably, for the (110) NiO surface we observe a remarkable electronic state characterized by an alternating charge-transfer and Mott-Hubbard character of the band gap in the surface and subsurface NiO layers, respectively. This novel form of electronic order stabilized by strong correlations is not driven by lattice reconstructions but of purely electronic origin. We notice the importance of orbital differentiation of the Ni e_g states to characterize the Mott-Hubbard insulating state of the (001) and (110) NiO surfaces. The unoccupied Ni e_g surface states are seen to split from the lower edge of the conduction band to form strongly localized states in the fundamental gap of bulk NiO. Our results for the surface energies of the (001) and (110) NiO surfaces show that the (001) facet of NiO has significantly lower energy. This implies that the relative stability of different surfaces, at least from a purely energetic point of view, does not depend on the presence or absence of magnetic order in NiO.

DOI: 10.1103/PhysRevB.103.165108

I. INTRODUCTION

The series of transition metal monoxides MnO, FeO, CoO, and NiO with an electronic configuration ranging from $3d^5$ to $3d^8$, respectively, has attracted much attention due to their diverse electronic and magnetic properties [1–5], allowing for a broad range of applications, e.g., in electronics and spintronics [6–9], energy storage [10–13], and heterogeneous catalysis [14–17]. At low temperature, these compounds exhibit a correlated Mott-Hubbard or charge-transfer insulating behavior with a large band gap of ∼2-4 eV, associated with a strong localization of the $3d$ electrons [18–22]. Below the Néel temperature, ranging from $T_N \sim 116$ to 523 K for MnO to NiO, respectively, these materials display an antiferromagnetic type-II long-range magnetic ordering and undergo a structural phase transition from a rocksalt cubic to a distorted rhombohedral (MnO and NiO) or monoclinic (FeO and CoO) phase [23].

Over the past decades particular attention has been devoted to understanding the nature of the band gap and excitation spectrum of MnO-NiO [18–22,24–30]. In fact, due to the strongly correlated nature of electron interactions between the $3d$ electrons, theoretical computations of the electronic structure of these materials using band-structure methods are particularly difficult. The Coulomb interactions may be modelled by including an onsite Hubbard parameter U to treat the effect of correlations in the partially filled $3d$ shell, e.g., within the so-called DFT + U method [25–27]. While these "beyond standard density functional theory (DFT)" methods often give a reliable description of the electronic properties such as band gaps, magnetic moments, and lattice displacements [30–35], these methods neglect electron dynamics and hence cannot capture correlated electron phenomena related to a Mott transition such as a coherence-incoherence crossover, quasiparticle behavior, and strong quasiparticle mass renormalization [18,19,36–38]. In fact, to determine

*Corresponding author: ivan.v.leonov@yandex.ru
†Corresponding author: silke.biermann@teorfys.lu.se

the electronic properties of these materials one needs to go beyond conventional band-structure methods to include dynamical correlation effects of the $3d$ electron (e.g., using DFT + U subject to dynamical symmetry-breaking spin and structural effects [28,29]).

It has been shown that the dynamical correlations and strong localization of the d (and f) electrons can be described by employing a DFT+ dynamical mean-field theory (DFT + DMFT) approach [36–38]. DFT + DMFT makes it possible to treat local correlation effects in a self-consistent, numerically exact way, providing a good description of the electronic and magnetic properties of correlated models and materials [36–63]. By using DFT + DMFT it becomes possible to compute the material-specific properties of complex correlated materials, e.g., to determine the electronic structure, magnetic state, and crystal structure of (para-) magnetic materials at finite temperatures, e.g., near the Mott transition [44–46,51–55].

The DFT + DMFT approach has been widely used to study the physical properties of the bulk structure of transition metal monoxides (TMOs), providing a quantitative description of the electronic, magnetic, and structural properties of these materials [43–53,55–60]. While the electronic structure and magnetic state of bulk TMOs are relatively well established nowadays (see, however, Refs. [64–66]), this is not the case for the different surface structures of metal oxides and their interfaces [1–5]. In fact, the electronic structure of a surface or interface can differ significantly from that of bulk, since their electronic states are responsible for a variety of novel (emerging) physical properties. In the case of surfaces, this affects, e.g., molecular adsorption and reactions that determine the catalytic processes at the surface [1–3]. In this respect, NiO is of particular interest among other TMOs due to its importance as catalysts for electrochemical applications, fuel cells, and batteries [10–17] (in addition to being a model system for understanding the Mott-Hubbard metal-insulator transition [18,19]).

The electronic properties of the nonpolar (001) and (110) and polar (111) NiO surfaces have been actively studied using different experimental techniques, such as x-ray photoemission spectroscopy (XPS), x-ray linear magnetic dichroism, electron-energy-loss spectroscopy (EELS), and scanning tunneling microscopy (STM), that give detailed information about the surface d-shell excitations and atomically resolved images of the surface states and reconstructions [1–5,67–74]. On the other hand, the effects of electron correlations and the electronic structure and magnetic properties of the NiO surfaces are still poorly understood. In practice, the electronic and magnetic properties of NiO surfaces have been studied using band-structure methods with the static mean-field Hubbard U treatment of correlation effects in the Ni $3d$ shell (e.g., within DFT + U) [75–84]. The strong localization of the $3d$ electrons and the finite temperature (para-) magnetic behavior of NiO still pose a challenge for an accurate description of the electronic properties of its surfaces using, e.g, DFT + DMFT [85,86], which is crucial for potential technical applications [10–17].

In this paper, we employ a multisite extension [41,42,54,87,88] of the DFT + DMFT method [89] implemented within a plane-wave pseudopotential formalism [51–54] to explore the effects of electronic correlations on the electronic properties of the nonpolar paramagnetic (PM) (001) and (110) surfaces of NiO. We study the electronic structure, magnetic properties, and surface energies of the (001) and (110) NiO with particular attention given to the effect of structural confinement and its influence on the strength of electronic correlations in the PM (001) and (110) NiO.

II. COMPUTATIONAL DETAILS

We perform a DFT + DMFT study of the electronic structure, magnetic properties, and surface energies of the clean (001) and (110) surfaces of the prototypical correlated insulator NiO. In DFT we employ the generalized gradient Perdew-Burke-Ernzerhof approximation (GGA) [90] within plane-wave pseudopotential formalism [91]. Our DFT + DMFT calculations explicitly include the Ni $3d$ and O $2p$ valence states by constructing a basis set of atomic-centered Wannier functions within the energy window spanned by the p-d band complex [92]. This makes it possible to take into account a charge transfer between the Ni $3d$ and O $2p$ states, accompanied by the strong onsite Coulomb correlations in the Ni $3d$ shell. In order to solve the realistic many-body problem within DMFT we use the continuous-time hybridization-expansion quantum Monte-Carlo (QMC) algorithm [93].

The DFT + DMFT calculations are performed in the *paramagnetic* state at an electronic temperature $T = 390\,\mathrm{K}$. We use the average Hubbard $U = 10\,\mathrm{eV}$ and Hund's exchange $J = 1\,\mathrm{eV}$, in accordance with previous works [25,52,57,94]. The Coulomb interaction U and Hund's J have been treated in the density-density approximation, with no spin-orbit coupling contribution. We employ the fully localized double-counting correction evaluated from the self-consistently determined local occupations to account for the electronic interactions already described by DFT. We use a fully self-consistent in charge density implementation of DFT + DMFT in order to take into account the effects of charge redistribution caused by electronic correlations and electron-lattice coupling [52,95]. In order to study the effects of structural confinement and relaxations we employ a multi-impurity-site extension of the DFT + DMFT method in order to treat correlations in the $3d$ bands of the structurally distinct Ni sites [41,42,54,87,88]. In addition, we perform structural relaxations of the surface and subsurface states of NiO within DFT. The DFT structural relaxation calculations are performed for the (fictitious) ferromagnetic (FM) state of NiO. For the relaxed structures the electronic properties of (001) and (110) PM NiO were evaluated within DFT + DMFT. The spectral functions were computed using the maximum entropy method and the Padé analytical continuation procedure.

III. RESULTS AND DISCUSSION

A. Electronic structure of (001) NiO

We begin with the electronic structure and equilibrium lattice volume calculations of bulk NiO in the paramagnetic state using DFT + DMFT [51,52,89]. In agreement with experiment, our calculations yield a correlated insulator with

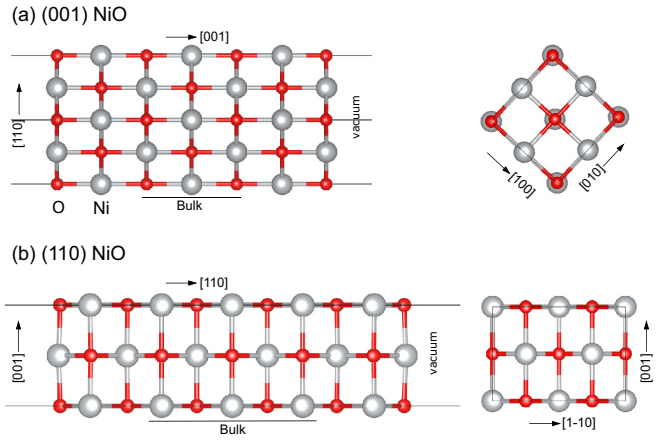

FIG. 1. (001) NiO (a) and (110) NiO slabs (b) used in the present DFT + DMFT calculations [96].

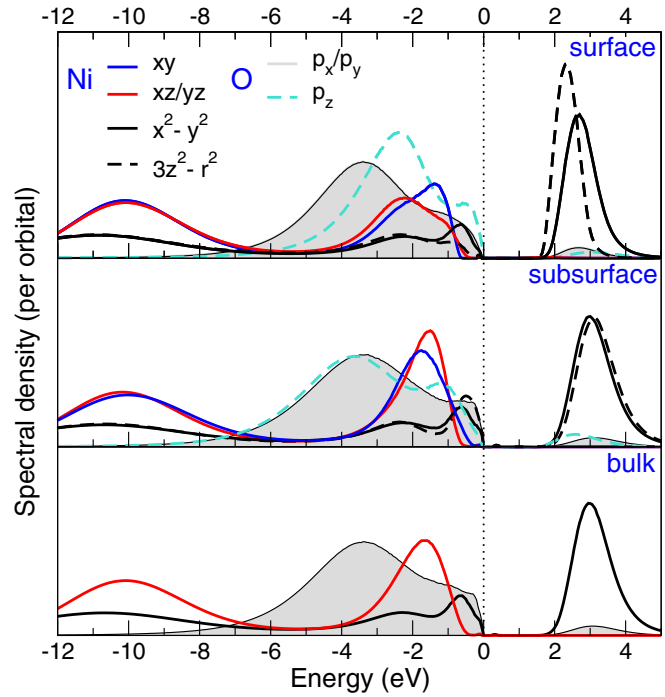

FIG. 2. Ni $3d$ and O $2p$ spectral functions calculated by DFT + DMFT for the relaxed (001) NiO at a temperature $T = 390$ K.

a large Ni d-d energy gap of about 2.9 eV and equilibrium lattice constant $a = 4.233$ Å (lattice volume of ∼128 a.u.^{3} and bulk modulus 187 GPa). The Ni^{2+} d^8 ions are in a high-spin ($S = 1$) state with an instantaneous local magnetic moment $\sqrt{\langle \hat{m}_z^2 \rangle} \simeq 1.83\ \mu_B$, corresponding to the fluctuating moment of 1.7 μ_B. The latter is evaluated as the imaginary-time average of the local spin susceptibilities $\chi(\tau) = \langle \hat{m}_z(\tau)\hat{m}_z(0)\rangle$ as $M_{\rm loc} = (k_B T \int \chi(\tau) d\tau)^{1/2}$. This result is in good agreement with the experimental estimate of 1.7–1.9 μ_B [97]. We note that the top of the valence band of NiO has a mixed Ni e_g and O $2p$ character, with a resonant peak in the filled Ni e_g band located at about 1 eV below the Fermi level. The latter can be ascribed to the formation of a Zhang-Rice bound state [98]. Our results suggest a mixture of a Mott-Hubbard Ni d-d and charge transfer type of the band gap which is caused by the effect of Coulomb correlations in the Ni $3d$ shell [20,21,24]. The bottom of the conduction band is mainly of the Ni $3d$ character with a broad paraboliclike Ni $4s$ band at the Brillouin zone Γ point.

Next, we use the equilibrium lattice constant obtained by DFT + DMFT for bulk NiO to construct the (001) symmetric slab consisting of 7-NiO monolayers (ML), with a thickness of about 12.59 Å and vacuum of ∼21 Å [see Fig. 1(a)]. Each ML in the slab contains two Ni sites. The top two NiO MLs are considered as a surface and subsurface, respectively, with 3-ML-thick NiO as a quasibulk. In our calculations we set the kinetic energy cutoff for the plane wave basis to 65 Ryd for the wave function and 650 Ryd for the charge density. We employ the three-impurity-site DFT + DMFT to treat structurally distinct the surface, subsurface, and quasibulk Ni $3d$ ions [99]. We first perform structural optimization of the surface and subsurface (001) NiO layers within FM GGA. It gives a small inward relaxation of the top ML of $\delta_{12} \simeq -2.5\%$ (0.054 Å) and a weak outward relaxation of the subsurface ML $\delta_{23} \sim 0.6\%$, with nearly absent surface buckling. Here, surface relaxations are characterized as a percent change of the spacing between layers i and j versus the equilibrium interlayer spacing d_0, $\delta_{ij} = (z_i^{\rm Ni} - z_j^{\rm Ni})/d_0$. We also find a small inward interplane relaxation between the first and third MLs, $\delta_{13} \sim -1.0\%$. Interestingly, the nomagnetic GGA yields –2.7% and –2.4% relaxation for the top and subsurface NiO-MLs, respectively, with a small surface buckling of ∼0.11 Å. At the same time, a structural optimization of the antiferromagnetic (001) surface of NiO within spin-polarized DFT + U (with $U - J = 7.0$ eV) [26,27,91] gives a relatively weak inward interplane relaxation of the surface layer $\delta_{12} \sim -1.05\%$ (∼0.022 Å), accompanied by a small outward relaxation of the subsurface ML $\delta_{23} \sim 0.5\%$ and inward relaxation between the first and third MLs, $\delta_{13} \sim -0.3\%$.

In Fig. 2 we show the orbitally-resolved spectral functions of (001) NiO obtained by DFT + DMFT for the relaxed within FM GGA surface of NiO. Our results for the unrelaxed bulk-terminated (001) NiO are shown in Supplemental Material Fig. S1 [100]. In accordance with experiment, we find a Mott-Hubbard insulator with a large (fundamental) energy gap of about 2.1 eV. The calculated local magnetic moments are 1.84, 1.82, and 1.82 μ_B for the surface, subsurface, and quasibulk Ni ions, respectively. The corresponding fluctuating moments are 1.78, 1.74, and 1.75 μ_B. Our results reveal a weak charge redistribution between the surface and bulk Ni sites. The total Wannier Ni $3d$ occupancies are nearly the same for all the Ni sites and differ by less than 0.03. In addition, we find no sizable distinction between the Ni $3z^2 - r^2$ and $x^2 - y^2$ orbital occupancies, which differ by less than 0.03 for all the Ni sites. At the same time, we observe a substantial splitting of the occupied O $2p$ and the empty Ni e_g bands at the surface caused by the effect of surface symmetry breaking (see the top panel of Fig. 2). It leads to a sizable reduction of the band gap from about 2.6 eV in the quasibulk to 2.1 eV at the surface. Moreover, surface relaxation (strain) is seen to result in a small increase of the band gap by less than ∼5%, from 2.0 to 2.1 eV. This result underlines the importance of the crystal-field splitting caused by the effect of surface truncation

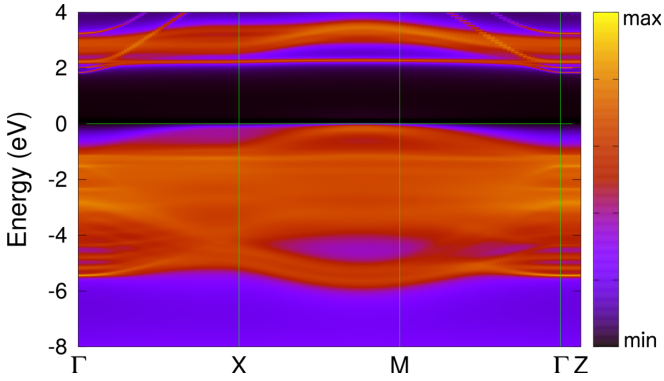

FIG. 3. The **k**-resolved total spectral function $A(\mathbf{k}, \omega)$ of (001) NiO along the Γ-X-M-Γ-Z lines in the Brillouin zone as obtained by DFT + DMFT at a temperature $T = 390$ K.

and relaxations for establishing the Mott insulating state of (001) NiO.

In the surface layer the top of the (001) NiO valence band shows a mixed Ni $x^2 - y^2$ and O $2p_z$ character, with a large contribution from the O $2p$ states, caused by the surface symmetry breaking and strain effects. Moreover, in the subsurface ML the top of the valence band has a mixed Ni $3z^2 - r^2$ and O $2p_x/p_y$ character. Our results therefore suggest a charge-transfer character of the (001) surface. Moreover, we also notice the importance of orbital differentiation of the Ni e_g states (for the surface and subsurface NiO-MLs) to characterize the correlated insulating state of (001) NiO. In addition to this, the unoccupied Ni $3z^2 - r^2$ surface states are seen to split from the lower edge of the conduction band and form a strongly localized (and dispersionless) band at about 2 eV above the E_F [see our results for the **k**-resolved spectra of (001) NiO in Fig. 3]. In contrast to this, at the top of the valence band, all bands merge with the continuum of bulk states.

We also calculated the local (dynamical) susceptibility $\chi(\tau) = \langle \hat{m}_z(\tau)\hat{m}_z(0)\rangle$ for the surface, subsurface, and quasi-bulk Ni^{2+} ions of PM (001) NiO. In Fig. 4(a) we display our results for the Ni e_g contributions in $\chi(\tau)$. τ denotes

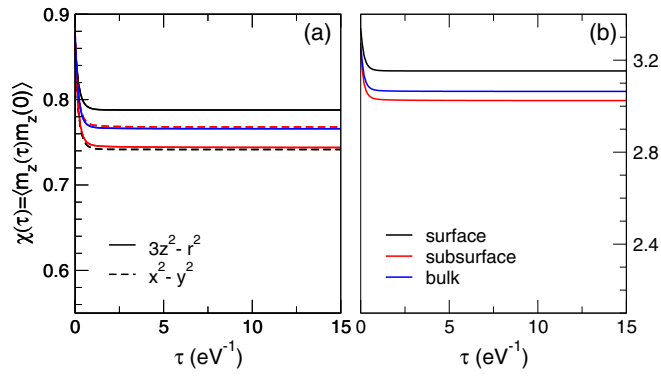

FIG. 4. Orbital-dependent (a) and total (b) local spin susceptibility $\chi(\tau) = \langle \hat{m}_z(\tau)\hat{m}_z(0)\rangle$ for the surface, subsurface, and bulk of paramagnetic (001) NiO as obtained by DFT + DMFT at an inverse temperature $\beta = 1/k_B T = 30\,\mathrm{eV}^{-1}$. Note that $\chi(\tau)$ is symmetric with respect to $\beta/2$, $\chi(\tau) \equiv \chi(\beta - \tau)$.

imaginary times. The value of this quantity around $\tau = \beta/2$ indicates the long time limit, and deviations from this value for small and large β indicate strong magnetic fluctuations. In the present case, all the e_g contributions are seen to be almost independent of τ, suggesting that the $3d$ electrons are localized to form fluctuating local moments. In fact, $\chi(\tau)$ is seen to be nearly constant and close to its maximal value $S = 1$ for the Ni e_g states. However, in the surface layer $\chi(\tau)$ is seen to be remarkably larger at all τ, implying higher localization of the surface e_g states. This leads to a higher charge-transfer character of the (001) NiO surface, while for the bulk our results suggest a mixture of a Mott-Hubbard d-d and charge transfer character of the band gap [20,21,24].

For the (001) NiO we compute the surface energy within DFT + DMFT as $\gamma \simeq (E^N_{\mathrm{slab}} - N E_{\mathrm{bulk}})/(2S)$ [101]. Here, E^N_{slab} is the total energy of an N-formula-unit slab of NiO. E_{bulk} is the total energy of bulk NiO per formula unit (f.u.). S is the surface area and the factor two accounts for the two surfaces in the slab unit cell. In order to minimize numerical differences between the bulk and the slab DFT + DMFT total energy calculations we adopt the same setup parameters within DFT + DMFT (such as kinetic energy cutoffs, **k**-point sampling, the shape of the unit cell, etc.) [102]. In particular, in our DFT + DMFT calculations we used a $10 \times 10 \times 8$ **k**-point grid for the (001) slab containing 14 f.u. of NiO. To estimate E_{bulk}, we computed the 4-f.u. cubic supercell of bulk NiO with a $10 \times 10 \times 28$ **k** grid. In both calculations we employed the same kinetic energy cutoffs for the wave functions (65 Ry) and for the charge density and potentials (650 Ry). Our result 59 meV/Å^2 is in good agreement with previous estimates in the antiferromagnetically ordered phase [78,80,83]. We note that the nonmagnetic GGA yields 44 meV/Å^2.

B. (110) NiO surface

We now turn to our results for the PM (110) NiO. To model (110) NiO we design the (110) 11-ML-thick slab with symmetry-equivalent surfaces. It is of 14.59 Å thick, with a vacuum spacer of about 21 Å [see Fig. 1(b)]. In our DFT + DMFT calculations, we treat the top three NiO MLs as surface, subsurface, and sub-subsurface layers, respectively. The remaining 5-ML-thick layer in the middle is taken as quasibulk NiO. We use the four-impurity-site extension of DFT + DMFT to treat the effect of correlations in the $3d$ shell of the structurally distinct Ni ions. In DFT the kinetic energy cutoff for the plane wave basis was set to 50 Ryd for the wave function and 500 Ryd for the charge density. All the calculations are performed in the local basis set determined by diagonalization of the corresponding Ni $3d$ occupation matrices. Structural optimization of the surface and two subsurface (110) NiO layers within FM GGA suggests that surface relaxations in (110) NiO are long range. It gives a large inward relaxation of the top layer of about -11.0% (-0.16 Å) accompanied by a sizable outward relaxation of the subsurface layer by 3.4%. The interplane relaxation between the first and third layer δ_{13} is about -3.8%, while $\delta_{15} \sim -2.9\%$. The above results are consistent with the results of a structural optimization of antiferromagnetic (110) NiO within DFT + U [91]. In particular, it gives a large inward interplane relaxation of the surface layer $\delta_{12} \sim -9.2\%$ (-0.138 Å), accompanied by a

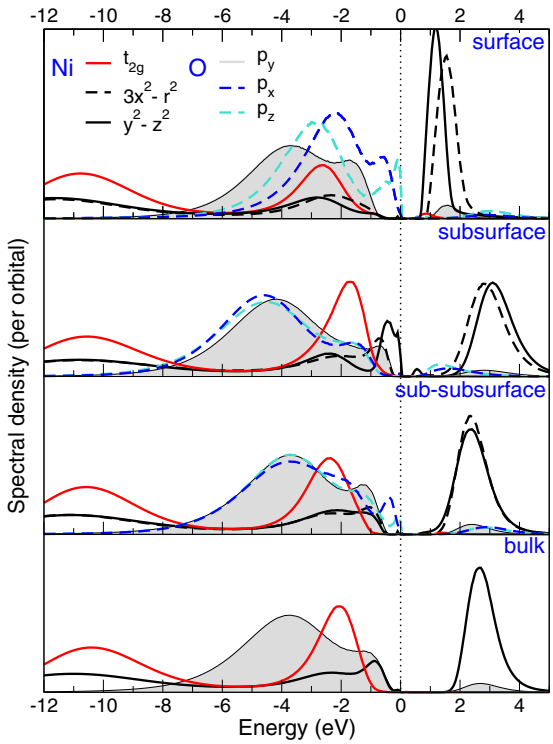

FIG. 5. Ni e_g and O $2p$ spectral functions of paramagnetic (110) NiO obtained by DFT + DMFT at a temperature $T = 390$ K.

large outward relaxation of the subsurface layer $\delta_{23} \sim 5.46\%$ (0.082 Å) and relatively weak inward relaxations between the first and third MLs, $\delta_{13} \sim -1.88\%$, and the third and fourth MLs, $\delta_{34} \sim -0.59\%$.

In Fig. 5 we summarize our results for the Ni $3d$ and O $2p$ spectral functions of PM (110) NiO. Our results for the **k**-resolved spectra are shown in Fig. 6. We obtain a Mott-Hubbard insulating solution with a relatively large band gap of 0.9 eV. Similarly to (001) NiO, we observe a weak variation of the local moments among the different Ni layers. In particular, the calculated local magnetic moments are 1.83, 1.79, 1.82, and 1.82 μ_B for the surface, two subsurfaces, and quasibulk Ni ions, respectively. Our estimate of the fluctuating moments is 1.77, 1.70, 1.73, and 1.75 μ_B. The Ni $3d$ occupancies are

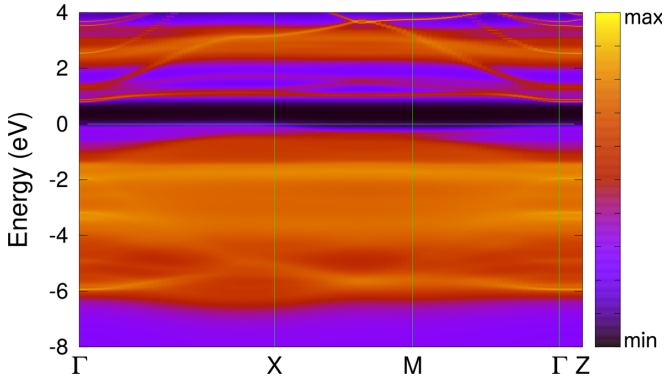

FIG. 6. The **k**-resolved total spectral function $A(\mathbf{k}, \omega)$ of (110) NiO along the Γ-X-M-Γ-Z lines in the Brillouin zone as obtained by DFT + DMFT at a temperature $T = 390$ K.

nearly the same for all the Ni sites, differing by less than 0.04. In addition, we observe no sizable difference between the Ni $3x^2 - r^2$ and $y^2 - z^2$ orbital occupancies in (110) NiO. The deviations are less than 0.03. Our analysis of the layer-dependent Ni $3d$ and O $2p$ spectral functions reveals a remarkable reduction of the band gap at the surface layer. In fact, it drops by about three times, from 2.9 eV in the quasibulk to 0.9 eV in the surface layer, in the relaxed (110) NiO. Most importantly, our result for the (fundamental) gap value of (110) NiO is more than twice smaller than that in the (001) NiO (2.1 eV). In close similarity to (001) NiO, structural relaxations of the surface result in an increase of the band gap from 0.8 to 0.9 eV.

Our results for the Ni $3d$ and O $2p$ spectral functions show a sizable splitting of the occupied O $2p$ and the empty Ni e_g bands (see Figs. 5 and 6). While at the top of the valence band, all bands merge with the continuum of bulk states, the unoccupied Ni e_g surface states are seen to split from the lower edge of the conduction band. These Ni e_g states form a localized band with a bandwidth of about 0.4 eV which appears in the bulk band gap at about 1 eV (see Fig. 6). Moreover, a detailed analysis of the top of the valence band reveals a large contribution of the O $2p$ states near the E_F, which are strongly mixed with the Ni $3d$ states. It is interesting to note, however, that the situation significantly differs from that in the (001) NiO or in bulk NiO. In fact, in contrast to the bulk and (001) NiO we observe that the top of the valence bands of (110) NiO has almost pure O $2p$ character at the surface and in the sub-subsurface layer, implying *a pure charge-transfer type* of the band gap of the (110) surface of NiO. In contrast to this, at the subsurface layer, it is nearly purely of Ni $3d$ $(y^2 - z^2)$ character, suggestive of a Mott-Hubbard type of the band gap in the subsurface layer of (110) NiO. Our results therefore document a novel electronic state characterized by an alternating pure charge-transfer and Mott-Hubbard character of the band gap in the surface and subsurface (110) NiO, respectively. This behavior suggests the absence of prominent Zhang-Rice physics at the (110) surface of NiO that reappear in bulk NiO [43,47,52]. We notice that this remarkable alternating charge-transfer and Mott-Hubbard state is robust with respect to the lattice reconstructions of the (110) surface as seen in the spectral function of the bulk-terminated (110) NiO (see Supplemental Material Fig. S2). This suggests that it is of purely electronic origin. Moreover, we notice a remarkable orbital differentiation of the Ni e_g states at the (sub)surface which seems to be important to characterize the transport properties of (110) NiO.

In Fig. 7 we display our results for the layer-dependent orbitally-resolved and total local susceptibility $\chi(\tau)$. We observe that all the e_g contributions are seen to be almost independent of τ, suggesting strongly localized nature of the Ni e_g states in (110) NiO. Similarly to (001) NiO the surface layer $\chi(\tau)$ is somewhat larger for all τ, implying a higher degree of localization of the surface e_g states. On the other hand, counterintuitive to this is the reduction of the band gap at the surface layer seen in the Ni $3d$ and O $2p$ spectral function for the (110) NiO surface, which is caused by charge-transfer effects.

We also calculate the surface energy of the relaxed (110) NiO using DFT + DMFT. In DFT + DMFT we used a 10 ×

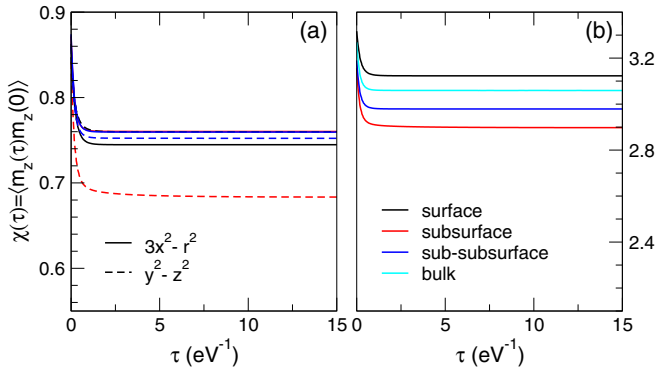

FIG. 7. Orbital-dependent (a) and total (b) local spin susceptibility $\chi(\tau) = \langle \hat{m}_z(\tau)\hat{m}_z(0)\rangle$ of paramagnetic (110) NiO as obtained by DFT + DMFT.

10×4 **k**-point grid for the 22-f.u. slab calculation of (110) NiO. In the bulk calculation we employed a 8-f.u. tetragonal supercell with a $10 \times 10 \times 24$ **k** grid. For the slab and bulk DFT + DMFT calculations the kinetic energy cutoffs were taken 50 Ry for the wave functions and 500 Ry for the charge density and potentials. Our result for the surface energy of (110) NiO 125 meV/Å^2 is substantially larger than that for the (001) NiO (59 meV/Å^2), implying that (001) NiO has significantly lower energy facet. The nonmagnetic GGA calculation gives 85 meV/Å^2 for (110) NiO.

IV. CONCLUSIONS

In conclusion, we have calculated the electronic structure, magnetic properties, and surfaces energies of the (001) and (110) surfaces of the prototypical correlated insulating material, PM NiO, using a multisite extension of the DFT + DMFT method. Our results reveal a complex interplay between electronic correlations and surface effects in NiO. We obtain that the electronic structure of the (001) and (110) NiO differs significantly from that of bulk NiO. In both (001) and (110) NiO we observe a sizable reduction of the band gap at the surface. The latter is most significant for the (110) NiO, from 2.9 in the quasibulk to 0.9 eV at the surface. Surface relaxations (surface strain) are seen to result in a remarkable increase of the band gap in comparison with the bulk-terminated NiO.

We observe a substantial splitting of the O $2p$ and Ni e_g bands at the surface caused by the effect of surface symmetry breaking. Our results suggest a charge-transfer character of the (001) and (110) surfaces of NiO. Most importantly, for the (110) NiO surface we observe a remarkable electronic state characterized by an alternating pure charge-transfer and Mott-Hubbard character of the band gap in the surface and subsurface NiO layers, respectively. This novel form of electronic order stabilized by strong correlations is not driven by lattice reconstructions but of purely electronic origin. Moreover, we notice the importance of orbital-differentiation of the Ni e_g states to characterize the Mott insulating state of the (001) and (110) NiO. The unoccupied Ni e_g surface states are seen to split from the lower edge of the conduction band to form strongly localized states in the fundamental gap of bulk NiO.

Our DFT + DMFT calculations reveal a remarkable difference between the electronic structure of the (001) and (110) NiO surfaces. For example, we obtain a large difference in their (fundamental) band gap value (by about a factor of two) due to the surface effects, ∼2.1 eV in the (001) and 0.9 eV for the (110) NiO surfaces. This suggests a higher catalytic activity of the (110) NiO surface than that of the (001) NiO surface. In agreement with previous estimates in the antiferromagnetically ordered phase, our DFT + DMFT calculations yield significantly different surface energies for the (001) and (110) NiO surfaces, of 59 and 125 meV/Å^2, respectively. Thus, the (001) NiO surface is found to have a significantly lower energy facet. We find that the effect of electron-electron correlations in NiO results in a sizable enhancement of the NiO surface energies by 34–48% with respect to the nonmagnetic GGA. Overall, our results for the electronic structure, magnetic properties, and surface energies of (001) and (110) NiO agree well with experimental data measured in the antiferromagnetic phase. Our results further reveal an intriguing independence of properties such as the energetical hierarchy of different surfaces of the presence or absence of antiferromagnetic order in NiO.

In accordance with previous studies of surfaces of strongly correlated materials, e.g., applications of DFT + DMFT to study $SrVO_3$ and $CaVO_3$ thin films [62,63] and to a $SrTiO_3$ surface [61], our results demonstrate the ability of multisite DFT + DMFT to compute the electronic structure and magnetic properties of transition metal oxide surfaces and thin films. The DFT + DMFT computations can be used to promote our understanding of the physics of surfaces, which are promising for applications. Further studies could, for example, deal with NiO deposited on $SrTiO_3$, elucidating the increased reactivity with water of such systems [103] or the design of highly active catalysts, e.g., for developing hybrid nickel-zinc and zinc-air batteries [13]. NiO is also being actively investigated for its resistive switching properties [104–106] for the description of which extensions of DFT + DMFT might also prove useful.

ACKNOWLEDGMENTS

We thank S. Backes, S. Panda, D. D. Sarma, and I. A. Abrikosov for valuable discussions. The DFT/DFT+U calculations and theoretical analysis of the electronic properties of (001) and (110) NiO were supported by the state assignment of Minobrnauki of Russia (theme "Electron" No. AAAA-A18-118020190098-5). The DFT + DMFT calculations of magnetic properties of (001) and (110) NiO were supported by Russian Science Foundation (Project No. 19-72-30043). S.B. acknowledges support from the European Research Council under Grant Agreement No. 617196, Project CORRELMAT, and from IDRIS/GENCI Orsay under Project No. t2021091393.

[1] H. H. Kung, *Transition Metal Oxides: Surface Chemistry and Catalysis* (Elsevier, Amsterdam, 1989), Vol. 45.

[2] V. E. Henrich and P. A. Cox, *The Surface Science of Metal Oxides* (Cambridge University Press, Cambridge, 1994).

[3] C. Noguera, *Physics and Chemistry of Oxide Surfaces* (Cambridge University Press, Cambridge, 1996).

[4] H.-J. Freund, H. Kuhlenbeck, and V. Staemmler, Oxide surfaces, Rep. Prog. Phys. **59**, 283 (1996).

[5] U. Kaiser, A. Schwarz, and R. Wiesendanger, Magnetic exchange force microscopy with atomic resolution, Nature (London) **446**, 522 (2007).

[6] Q. Liu, Q. Chen, Q. Zhang, Y. Xiao, X. Zhong, G. Dong, M.-P. Delplancke-Ogletree, H. Terryn, K. Baert, F. Reniers, and X. Diao, In situ electrochromic efficiency of a nickel oxide thin film: origin of electrochemical process and electrochromic degradation, J. Mater. Chem. C **6**, 646 (2018).

[7] W. Lin, K. Chen, S. Zhang, and C. L. Chien, Enhancement of Thermally Injected Spin Current through an Antiferromagnetic Insulator, Phys. Rev. Lett. **116**, 186601 (2016).

[8] E. Aytan, B. Debnath, F. Kargar, Y. Barlas, M. M. Lacerda, J. X. Li, R. K. Lake, J. Shi, and A. A. Balandin, Spin-phonon coupling in antiferromagnetic nickel oxide, Appl. Phys. Lett. **111**, 252402 (2017).

[9] M. Dabrowski, T. Nakano, D. M. Burn, A. Frisk, D. G. Newman, C. Klewe, Q. Li, M. Yang, P. Shafer, E. Arenholz, T. Hesjedal, G. van der Laan, Z. Q. Qiu, and R. J. Hicken, Coherent Transfer of Spin Angular Momentum by Evanescent Spin Waves within Antiferromagnetic NiO, Phys. Rev. Lett. **124**, 217201 (2020).

[10] P. L. S. G. Poizot, S. Laruelle, S. Grugeon, L. Dupont, and J. M. Tarascon, Nano-sized transition-metal oxides as negative-electrode materials for lithium-ion batteries, Nature (London) **407**, 496 (2000).

[11] M. V. Reddy, G. V. Subba Rao, and B. V. R. Chowdari, Metal oxides and oxysalts as anode materials for Li ion batteries, Chem. Rev. **113**, 5364 (2013).

[12] D. Su, M. Ford, and G. Wang, Mesoporous NiO crystals with dominantly exposed (110) reactive facets for ultrafast lithium storage, Sci. Rep. **2**, 924 (2012).

[13] D. U. Lee, J. Fu, M. G. Park, H. Liu, A. G. Kashkooli, and Z. Chen, Self-assembled NiO/Ni$(OH)_2$ nanoflakes as active material for high-power and high-energy hybrid rechargeable battery, Nano Lett. **16**, 1794 (2016).

[14] W. Zhao, M. Bajdich, S. Carey, and A. Vojvodic, Water dissociative adsorption on NiO(111): Energetics and structure of the hydroxylated surface, ACS Catal. **6**, 7377 (2016).

[15] A. Nelson, K. E. Fritz, S. Honrao, R. G. Hennig, R. D. Robinson, and J. Suntivich, Increased activity in hydrogen evolution electrocatalysis for partial anionic substitution in cobalt oxysulfide nanoparticles, J. Mater. Chem. A **4**, 2842 (2016).

[16] R. Poulain, A. Klein, and J. Proost, Electrocatalytic properties of (001)-, (110)-, and (111)-oriented NiO thin films toward the oxygen evolution reaction, J. Phys. Chem. C **122**, 22252 (2018).

[17] S. Gong, A. Wang, Y. Wang, H. Liu, N. Han, and Y. Chen, Heterostructured Ni/NiO nanocatalysts for ozone decomposition, ACS Appl. Nano Mater. **3**, 597 (2020).

[18] N. F. Mott, *Insulator Transitions* (Taylor & Francis, London, 1990).

[19] M. Imada, A. Fujimori, and Y. Tokura, Metal-insulator transitions, Rev. Mod. Phys. **70**, 1039 (1998).

[20] G. A. Sawatzky and J. W. Allen, Magnitude and Origin of the Band Gap in NiO, Phys. Rev. Lett. **53**, 2339 (1984).

[21] J. Zaanen, G. A. Sawatzky, and J. W. Allen, Band Gaps and Electronic Structure of Transition-Metal Compounds, Phys. Rev. Lett. **55**, 418 (1985).

[22] Z.-X. Shen, R. S. List, D. S. Dessau, B. O. Wells, O. Jepsen, A. J. Arko, R. Barttlet, C. K. Shih, F. Parmigiani, J. C. Huang, and P. A. P. Lindberg, Electronic structure of NiO: Correlation and band effects, Phys. Rev. B **44**, 3604 (1991).

[23] W. L. Roth, Magnetic structures of MnO, FeO, CoO, and NiO, Phys. Rev. **110**, 1333 (1958).

[24] T. M. Schuler, D. L. Ederer, S. Itza-Ortiz, G. T. Woods, T. A. Callcott, and J. C. Woicik, Character of the insulating state in NiO: A mixture of charge-transfer and Mott-Hubbard character, Phys. Rev. B **71**, 115113 (2005).

[25] V. I. Anisimov, J. Zaanen, and O. K. Andersen, Band theory and Mott insulators: Hubbard U instead of Stoner I, Phys. Rev. B **44**, 943 (1991); V. I. Anisimov, I. V. Solovyev, M. A. Korotin, M. T. Czyzyk, and G. A. Sawatzky, Density-functional theory and NiO photoemission spectra, *ibid.* **48**, 16929 (1993).

[26] S. L. Dudarev, G. A. Botton, S. Y. Savrasov, C. J. Humphreys and A. P. Sutton, Electron-energy-loss spectra and the structural stability of nickel oxide: An LSDA + U study, Phys. Rev. B **57**, 1505 (1998).

[27] M. Cococcioni and S. de Gironcoli, Linear response approach to the calculation of the effective interaction parameters in the LDA + U method, Phys. Rev. B **71**, 035105 (2005).

[28] G. Trimarchi, Z. Wang, and A. Zunger, Polymorphous band structure model of gapping in the antiferromagnetic and paramagnetic phases of the Mott insulators MnO, FeO, CoO, and NiO, Phys. Rev. B **97**, 035107 (2018); J. Varignon, M. Bibes, and A. Zunger, Origin of band gaps in 3d perovskite oxides, Nat. Commun. **10**, 1658 (2019).

[29] Z. Wang, O. Malyi, X. Zhao, and A. Zunger, Mass enhancement in 3d and s-p perovskites from symmetry breaking, arXiv:2006.00199.

[30] V. Potapkin, L. Dubrovinsky, I. Sergueev, M. Ekholm, I. Kantor, D. Bessas *et al.*, Magnetic interactions in NiO at ultrahigh pressure, Phys. Rev. B **93**, 201110(R) (2016).

[31] A. Schrön, C. Rödl, and F. Bechstedt, Crystalline and magnetic anisotropy of the 3d-transition metal monoxides MnO, FeO, CoO, and NiO, Phys. Rev. B **86**, 115134 (2012).

[32] C. Rödl and F. Bechstedt, Optical and energy-loss spectra of the antiferromagnetic transition metal oxides MnO, FeO, CoO, and NiO including quasiparticle and excitonic effects, Phys. Rev. B **86**, 235122 (2012).

[33] H. Jiang, R. I. Gomez-Abal, P. Rinke, and M. Scheffler, First-principles modeling of localized d states with the GW@LDA + U approach, Phys. Rev. B **82**, 045108 (2010).

[34] K. Karlsson, F. Aryasetiawan, and O. Jepsen, Method for calculating the electronic structure of correlated materials from a truly first-principles LDA + U scheme, Phys. Rev. B **81**, 245113 (2010).

[35] P. Liu, C. Franchini, M. Marsman, and G. Kresse, Assessing model-dielectric-dependent hybrid functionals on the antiferromagnetic transition-metal monoxides MnO, FeO, CoO, and NiO, J. Phys.: Condens. Matter **32**, 015502 (2020).

[36] A. Georges, G. Kotliar, W. Krauth, and M. J. Rozenberg, Dynamical mean-field theory of strongly correlated fermion systems and the limit of infinite dimensions, Rev. Mod. Phys. **68**, 13 (1996); G. Kotliar, S. Y. Savrasov, K. Haule, V. S.

Oudovenko, O. Parcollet, and C. A. Marianetti, Electronic structure calculations with dynamical mean-field theory, *ibid.* **78**, 865 (2006).

[37] R. C. Kent and G. Kotliar, Toward a predictive theory of correlated materials, Science **361**, 348 (2018).

[38] S. Biermann, *Topics in Current Chemistry* (Springer, Berlin, Heidelberg, 2014), Vol. 347, pp. 303–345.

[39] S. Biermann, A. Dallmeyer, C. Carbone, W. Eberhardt, C. Pampuch, O. Rader, M. I. Katsnelson, A. I. Lichtenstein, Observation of Hubbard bands in γ-manganese, JETP Lett. **80**, 612 (2004).

[40] E. Pavarini, S. Biermann, A. Poteryaev, A. I. Lichtenstein, A. Georges, and O. K. Andersen, Mott Transition and Suppression of Orbital Fluctuations in Orthorhombic $3d^1$ Perovskites, Phys. Rev. Lett. **92**, 176403 (2004).

[41] A. I. Poteryaev, A. I. Lichtenstein, and G. Kotliar, Nonlocal Coulomb Interactions and Metal-Insulator Transition in Ti_2O_3: A Cluster LDA+DMFT Approach, Phys. Rev. Lett. **93**, 086401 (2004).

[42] S. Biermann, A. I. Poteryaev, A. I. Lichtenstein, and A. Georges, Dynamical Singlets and Correlation-Assisted Peierls Transition in VO_2, Phys. Rev. Lett. **94**, 026404 (2005).

[43] J. Kunes, V. I. Anisimov, A. V. Lukoyanov, and D. Vollhardt, Local correlations and hole doping in NiO: A dynamical mean-field study, Phys. Rev. B **75**, 165115 (2007); J. Kunes, V. I. Anisimov, S. L. Skornyakov, A. V. Lukoyanov, and D. Vollhardt, NiO: Correlated Band Structure of a Charge-Transfer Insulator, Phys. Rev. Lett. **99**, 156404 (2007).

[44] J. Kunes, A. V. Lukoyanov, V. I. Anisimov, R. T. Scalettar, and W. E. Pickett, Collapse of magnetic moment drives the Mott transition in MnO, Nat. Mater. **7**, 198 (2008).

[45] A. O. Shorikov, Z. V. Pchelkina, V. I. Anisimov, S. L. Skornyakov, and M. A. Korotin, Orbital-selective pressure-driven metal to insulator transition in FeO from dynamical mean-field theory, Phys. Rev. B **82**, 195101 (2010).

[46] K. Ohta, R. E. Cohen, K. Hirose, K. Haule, K. Shimizu, and Y. Ohishi, Experimental and Theoretical Evidence for Pressure-Induced Metallization in FeO with Rocksalt-Type Structure, Phys. Rev. Lett. **108**, 026403 (2012).

[47] Q. Yin, A. Gordienko, X. Wan, S. Y. Savrasov, Calculated Momentum Dependence of Zhang-Rice States in Transition Metal Oxides, Phys. Rev. Lett. **100**, 066406 (2008).

[48] P. Thunström, I. Di Marco, and O. Eriksson, Electronic Entanglement in Late Transition Metal Oxides, Phys. Rev. Lett. **109**, 186401 (2012).

[49] K. Byczuk, J. Kunes, W. Hofstetter, and D. Vollhardt, Quantification of Correlations in Quantum Many-Particle Systems, Phys. Rev. Lett. **108**, 087004 (2012).

[50] I. A. Nekrasov, N. S. Pavlov, M. V. Sadovskii, Consistent LDA'+DMFT – an unambiguous way to avoid double counting problem: NiO test, JETP Lett. **95**, 581 (2012); Consistent LDA'+DMFT approach to electronic structure of transition metal oxides: charge transfer insulators and correlated metals, J. Exp. Theor. Phys. **116**, 620 (2013).

[51] I. Leonov, Metal-insulator transition and local-moment collapse in FeO under pressure, Phys. Rev. B **92**, 085142 (2015); I. Leonov, A. V. Ponomareva, R. Nazarov, and I. A. Abrikosov, Pressure-induced spin-state transition of iron in magnesiowüstite (Fe, Mg)O, *ibid.* **96**, 075136 (2017).

[52] I. Leonov, L. Pourovskii, A. Georges, and I. A. Abrikosov, Magnetic collapse and the behavior of transition metal oxides at high pressure, Phys. Rev. B **94**, 155135 (2016); I. Leonov, A. O. Shorikov, V. I. Anisimov, and I. A. Abrikosov, Emergence of quantum critical charge and spin-state fluctuations near the pressure-induced Mott transition in MnO, FeO, CoO, and NiO, *ibid.* **101**, 245144 (2020).

[53] E. Greenberg, R. Nazarov, A. Landa, J. Ying, R. Q. Hood, B. Hen, R. Jeanloz, V. B. Prakapenka, V. V. Struzhkin, G. Kh. Rozenberg, and I. Leonov, Phase transitions and spin-state of iron in FeO at the conditions of Earth's deep interior, arXiv:2004.00652.

[54] E. Greenberg, I. Leonov, S. Layek, Z. Konopkova, M. P. Pasternak, L. Dubrovinsky, R. Jeanloz, I. A. Abrikosov, and G. Kh. Rozenberg, Pressure-Induced Site-Selective Mott Insulator-Metal Transition in Fe_2O_3, Phys. Rev. X **8**, 031059 (2018); I. Leonov, G. Kh. Rozenberg, and I. A. Abrikosov, Charge disproportionation and site-selective local magnetic moments in the post-perovskite-type Fe_2O_3 under ultra-high pressures, npj Comput. Mater. **5**, 90 (2019).

[55] N. Lanatá, T.- H. Lee, Y.-X. Yao, V. Stevanović, and V. Dobrosavljević, Connection between Mott physics and crystal structure in a series of transition metal binary compounds, npj Comput. Mater. **5**, 30 (2019).

[56] S. K. Panda, B. Pal, S. Mandal, M. Gorgoi, S. Das, I. Sarkar *et al.*, High photon energy spectroscopy of NiO: Experiment and theory, Phys. Rev. B **93**, 235138 (2016).

[57] S. K. Panda, H. Jiang, and S. Biermann, Pressure dependence of dynamically screened Coulomb interactions in NiO: Effective Hubbard, Hund, intershell, and intersite components, Phys. Rev. B **96**, 045137 (2017).

[58] F. Lechermann, W. Körner, D. F. Urban, and C. Elsässer, Interplay of charge-transfer and Mott-Hubbard physics approached by an efficient combination of self-interaction correction and dynamical mean-field theory, Phys. Rev. B **100**, 115125 (2019).

[59] S. Mandal, K. Haule, K. M. Rabe, and D. Vanderbilt, Influence of magnetic ordering on the spectral properties of binary transition metal oxides, Phys. Rev. B **100**, 245109 (2019).

[60] E. Koemets, I. Leonov, M. Bykov, E. Bykova, S. Chariton *et al.*, Revealing the Complex Nature of Bonding in the Binary High-Pressure Compound FeO_2, Phys. Rev. Lett. **126**, 106001 (2021).

[61] Z. Zhong, A. Tóth, and K. Held, Theory of spin-orbit coupling at $LaAlO_3/SrTiO_3$ interfaces and $SrTiO_3$ surfaces, Phys. Rev. B **87**, 161102(R) (2013).

[62] Z. Zhong, M. Wallerberger, J. M. Tomczak, C. Taranto, N. Parragh, A. Toschi, G. Sangiovanni, and K. Held, Electronics with Correlated Oxides: $SrVO_3/SrTiO_3$ as a Mott Transistor, Phys. Rev. Lett. **114**, 246401 (2015).

[63] S. Beck, G. Sclauzero, U. Chopra, and C. Ederer, Metal-insulator transition in $CaVO_3$ thin films: Interplay between epitaxial strain, dimensional confinement, and surface effects, Phys. Rev. B **97**, 075107 (2018).

[64] M. Karolak, G. Ulm, T. Wehling, V. Mazurenko, A. Poteryaev, and A. Lichtenstein, Double counting in LDA+DMFT – the example of NiO, J. Electron. Spectrosc. Relat. Phenom. **181**, 11 (2010).

[65] T. Haupricht, J. Weinen, A. Tanaka, R. Gierth, S. G. Altendorf, Y.-Y. Chin *et al.*, Local correlations, non-local screening, multiplets, and band formation in NiO, arXiv:1210.6675.

[66] C.-Y. Kuo, T. Haupricht, J. Weinen, H. Wu, K.-D. Tsuei, M. W. Haverkort, A. Tanaka, and L. H. Tjeng, Challenges from experiment: Electronic structure of NiO, Eur. Phys. J.: Spec. Top. **226**, 2445 (2017).

[67] B. Fromme, M. Möller, Th. Anschütz, C. Bethke, and E. Kisker, Electron-Exchange Processes in the Excitations of NiO(001) Surface *d* States, Phys. Rev. Lett. **77**, 1548 (1996).

[68] D. Alders, L. H. Tjeng, F. C. Voogt, T. Hibma, G. A. Sawatzky, C. T. Chen, J. Vogel, M. Sacchi, and S. Iacobucci, Temperature and thickness dependence of magnetic moments in NiO epitaxial films, Phys. Rev. B **57**, 11623 (1998).

[69] J. Stöhr, A. Scholl, T. J. Regan, S. Anders, J. Lüning, M. R. Scheinfein, H. A. Padmore, and R. L. White, Images of the Antiferromagnetic Structure of a NiO(001) Surface by Means of X-Ray Magnetic Linear Dichroism Spectromicroscopy, Phys. Rev. Lett. **83**, 1862 (1999).

[70] A. Barbier, C. Mocuta, H. Kuhlenbeck, K. F. Peters, B. Richter, and G. Renaud, Atomic Structure of the Polar NiO(111)-p (2×2) Surface, Phys. Rev. Lett. **84**, 2897 (2000); A. Barbier, C. Mocuta, and G. Renaud, Structure, transformation, and reduction of the polar NiO (111) surface, Phys. Rev. B **62**, 16056 (2000).

[71] H. Ohldag, A. Scholl, F. Nolting, S. Anders, F. U. Hillebrecht, and J. Stöhr, Spin Reorientation at the Antiferromagnetic NiO(001) Surface in Response to an Adjacent Ferromagnet, Phys. Rev. Lett. **86**, 2878 (2001).

[72] F. U. Hillebrecht, H. Ohldag, N. B. Weber, C. Bethke, U. Mick, M. Weiss, and J. Bahrdt, Magnetic Moments at the Surface of Antiferromagnetic NiO(001), Phys. Rev. Lett. **86**, 3419 (2001).

[73] L. Soriano, I. Preda, A. Gutiérrez, S. Palacin, M. Abbate, and A. Vollmer, Surface effects in the Ni $2p$ x-ray photoemission spectra of NiO, Phys. Rev. B **75**, 233417 (2007).

[74] F. Pielmeier and F. J. Giessibl, Spin Resolution and Evidence for Superexchange on NiO(001) Observed by Force Microscopy, Phys. Rev. Lett. **110**, 266101 (2013).

[75] M. R. Castell, S. L. Dudarev, G. A. D. Briggs, and A. P. Sutton, Unexpected differences in the surface electronic structure of NiO and CoO observed by STM and explained by first-principles theory, Phys. Rev. B **59**, 7342 (1999).

[76] J.-T. Hoeft, M. Kittel, M. Polcik, S. Bao, R. L. Toomes, J.-H. Kang, D. P. Woodruff, M. Pascal, and C. L. A. Lamont, Molecular Adsorption Bond Lengths at Metal Oxide Surfaces: Failure of Current Theoretical Methods, Phys. Rev. Lett. **87**, 086101 (2001).

[77] D. Ködderitzsch, W. Hergert, W. M. Temmerman, Z. Szotek, A. Ernst, and H. Winter, Exchange interactions in NiO and at the NiO(001) surface, Phys. Rev. B **66**, 064434 (2002).

[78] O. Bengone, M. Alouani, J. Hugel, P. Blöchl, LDA + U calculated electronic and structural properties of NiO (001) and NiO(111) $p(2 \times 2)$ surfaces, Comput. Mater. Sci. **24**, 192 (2002).

[79] A. Wander, I. J. Bush, and N. M. Harrison, Stability of rocksalt polar surfaces: An *ab initio* study of MgO (111) and NiO (111), Phys. Rev. B **68**, 233405 (2003).

[80] A. Rohrbach, J. Hafner, and G. Kresse, Molecular adsorption on the surface of strongly correlated transition-metal oxides: A case study for CO/NiO(100), Phys. Rev. B **69**, 075413 (2004); A. Rohrbach and J. Hafner, Molecular adsorption of NO on NiO(001): DFT and DFT + U calculations, *ibid.* **71**, 045405 (2005).

[81] A. M. Ferrari, C. Pisani, F. Cinquini, L. Giordano, and G. Pacchioni, Cationic and anionic vacancies on the NiO(001) surface: DFT+U and hybrid functional density functional theory calculations, J. Chem. Phys. **127**, 174711 (2007).

[82] N. Yu, W.-B. Zhang, N. Wang, Y.-F. Wang, and B.-Y. Tang, Water Adsorption on a NiO(001) Surface: A GGA + U Study, J. Phys. Chem. C **112**, 452 (2008).

[83] A. Schrön, M. Granovskij, and F. Bechstedt, Influence of on-site Coulomb interaction U on properties of MnO(001)2×1 and NiO(001)2×1 surfaces, J. Phys.: Condens. Matter **25**, 094006 (2013); A. Schrön and F. Bechstedt, Spin-dependent properties and images of MnO, FeO, CoO, and NiO(001) surfaces, Phys. Rev. B **92**, 165112 (2015).

[84] V. S. C. Kolluru and R. G. Hennig, Role of magnetism on transition metal oxide surfaces in vacuum and solvent, Phys. Rev. Materials **4**, 045803 (2020).

[85] M. Potthoff and W. Nolting, Surface metal-insulator transition in the Hubbard model, Phys. Rev. B **59**, 2549 (1999); Metallic surface of a Mott insulator-Mott insulating surface of a metal, **60**, 7834 (1999).

[86] M. Potthoff, Metal-Insulator Transitions at Surfaces, Adv. Solid State Phys. **42**, 121 (2002).

[87] J.-Z. Ma, A. van Roekeghem, P. Richard, Z.-H. Liu, H. Miao, L.-K. Zeng *et al.*, Correlation-Induced Self-Doping in the Iron-Pnictide Superconductor $Ba_2Ti_2Fe_2As_4O$, Phys. Rev. Lett. **113**, 266407 (2014).

[88] P. Delange, T. Ayral, S. I. Simak, M. Ferrero, O. Parcollet, S. Biermann, and L. Pourovskii, Large effects of subtle electronic correlations on the energetics of vacancies in α-Fe, Phys. Rev. B **94**, 100102(R) (2016).

[89] The DFT+DMFT code employed in this study is available upon request from the corresponding author I.L. (ivan.v.leonov@yandex.ru).

[90] J. P. Perdew, K. Burke, and M. Ernzerhof, Generalized Gradient Approximation Made Simple, Phys. Rev. Lett. **77**, 3865 (1996).

[91] S. Baroni, S. de Gironcoli, A. Dal Corso, and P. Giannozzi, Rev. Mod. Phys. **73**, 515 (2001); P. Giannozzi, S. Baroni, N. Bonini, M. Calandra, R. Car *et al.*, QUANTUM ESPRESSO: A modular and open-source software project for quantum simulations of materials, J. Phys.: Condens. Matter **21**, 395502 (2009).

[92] N. Marzari, A. A. Mostofi, J. R. Yates, I. Souza, and D. Vanderbilt, Maximally localized Wannier functions: Theory and applications, Rev. Mod. Phys. **84**, 1419 (2012); V. I. Anisimov, D. E. Kondakov, A. V. Kozhevnikov, I. A. Nekrasov, Z. V. Pchelkina, J. W. Allen *et al.*, Full orbital calculation scheme for materials with strongly correlated electrons, Phys. Rev. B **71**, 125119 (2005); G. Trimarchi, I. Leonov, N. Binggeli, Dm. Korotin, and V. I. Anisimov, LDA+DMFT implemented with the pseudopotential plane-wave approach, J. Phys.: Condens. Matter **20**, 135227 (2008).

[93] E. Gull, A. J. Millis, A. I. Lichtenstein, A. N. Rubtsov, M. Troyer, and P. Werner, Continuous-time Monte Carlo methods for quantum impurity models, Rev. Mod. Phys. **83**, 349 (2011).

[94] R. Sakuma and F. Aryasetiawan, First-principles calculations of dynamical screened interactions for the transition metal oxides MO (M = Mn, Fe, Co, Ni), Phys. Rev. B **87**, 165118 (2013).

[95] For a review, see, e.g., L. V. Pourovskii, B. Amadon, S. Biermann, and A. Georges, Self-consistency over the charge density in dynamical mean-field theory: A linear muffin-tin implementation and some physical implications, Phys. Rev. B **76**, 235101 (2007); K. Haule, Quantum Monte Carlo impurity solver for cluster dynamical mean-field theory and electronic structure calculations with adjustable cluster base, *ibid.* **75**, 155113 (2007); B. Amadon, F. Lechermann, A. Georges, F. Jollet, T. O. Wehling, and A. I. Lichtenstein, Plane-wave based electronic structure calculations for correlated materials using dynamical mean-field theory and projected local orbitals, *ibid.* **77**, 205112 (2008); M. Aichhorn, L. Pourovskii, V. Vildosola, M. Ferrero, O. Parcollet, T. Miyake, A. Georges, and S. Biermann, Dynamical mean-field theory within an augmented plane-wave framework: Assessing electronic correlations in the iron pnictide LaFeAsO, *ibid.* **80**, 085101 (2009); B. Amadon, A self-consistent DFT+DMFT scheme in the projector augmented wave method: Applications to cerium, Ce_2O_3 and Pu_2O_3 with the Hubbard I solver and comparison to DFT + U, J. Phys.: Condens. Matter **24**, 075604 (2012).

[96] K. Momma and F. Izumi, VESTA 3 for three-dimensional visualization of crystal, volumetric and morphology data, J. Appl. Crystallogr. **44**, 1272 (2011).

[97] H. A. Alperin, J. Phys. Soc. Jpn. Suppl. B **17**, 12 (1962); B. E. F. Fender, A. J. Jacobson, and F. A. Wedgwood, Covalency Parameters in MnO, α-MnS, and NiO, J. Chem. Phys. **48**, 990 (1968); A. K. Cheetham and D. A. O. Hope, Magnetic ordering and exchange effects in the antiferromagnetic solid solutions $Mn_xNi_{1-x}O$, Phys. Rev. B **27**, 6964 (1983).

[98] F. C. Zhang and T. M. Rice, Effective hamiltonian for the superconducting Cu oxides, Phys. Rev. B **37**, 3759 (1988).

[99] S. Keshavarz, Y. O. Kvashnin, I. Di Marco, A. Delin, M. I. Katsnelson, A. I. Lichtenstein, and O. Eriksson, Layer-resolved magnetic exchange interactions of surfaces of late 3d elements: Effects of electronic correlations, Phys. Rev. B **92**, 165129 (2015).

[100] See Supplemental Material at http://link.aps.org/supplemental/10.1103/PhysRevB.103.165108 for additional results supporting our conclusions.

[101] N. E. Singh-Miller and N. Marzari, Surface energies, work functions, and surface relaxations of low-index metallic surfaces from first principles, Phys. Rev. B **80**, 235407 (2009).

[102] We note that even on the DFT or DFT + U level, it is difficult to estimate the surface energies reliably. In fact, it requires estimating a relatively small total energy difference between the slab and bulk total energies, which depend sensitively upon fine details of the total energy calculations (kinetic energy cutoffs, **k**-points sampling, etc.). In our DFT+DMFT calculations (for given cutoffs in kinetic energy, charge density, Matsubara frequencies, and **k**-points sampling) the total energy is typically converged to $\sim 1-2$ meV/f.u., which makes the stochastic errors in QMC to be essentially negligible. At the same time, we had to converge the DFT+DMFT results with different **k**-points sets.

[103] S. Gerhold, M. Riva, Z. Wang, R. Bliem, M. Wagner, J. Osiecki, K. Schulte, M. Schmid, and U. Diebold, Nickel-Oxide-Modified $SrTiO_3(110)$-(4×1) Surfaces and Their Interaction with Water, J. Phys. Chem. C **119**, 20481 (2015).

[104] A. Sawa, Resistive Switching in transition metal oxides, Mater. Today **11**, 28 (2008).

[105] K. Kinoshtia, T. Okutani, H. Tanaka, T. Hinoki, K. Yazawa, K. Ohmi, and S. Kishida, Opposite bias polarity dependence of resistive switching in n-type Ga-doped-ZnO and p-type NiO thin films, Appl. Phys. Lett. **96**, 143505 (2010).

[106] K. M. Kim, D. S. Jeong, and C. S. Hwang, Nanofilamentary resistive switching in binary oxide system; a review on the present status and outlook, Nanotech. **22**, 254002 (2011).